THE ASTROPHYSICAL JOURNAL, 272:383–389, 1983 September 15

VLBI MAPS OF 3C 273 AND 3C 345 AT 2.3 GHz

M. H. COHEN, S. C. UNWIN, K. R. LIND, A. T. MOFFET, AND R. S. SIMON
Owens Valley Radio Observatory, California Institute of Technology
P. N. WILKINSON AND R. E. SPENCER
Nuffield Radio Astronomy Laboratories, Jodrell Bank
R. S. BOOTH
Onsala Space Observatory
G. D. NICOLSON
National Institute for Telecommunications Research, Johannesburg
AND
A. E. NIELL AND L. E. YOUNG
Jet Propulsion Laboratory
Received 1982 December 3; accepted 1983 March 8

ABSTRACT

Maps of the quasars 3C 273 and 3C 345 made at 2.3 GHz with an eight station VLBI array are presented. Five compact components spanning 45 milli-arcsec are seen in 3C 273, and four are seen in 3C 345. Comparisons with maps at higher and lower frequencies show that in both sources the core, which dominates the high-frequency "core-jet" structure, is strongly self-absorbed at 2.3 GHz and below. The jet components have flat spectra, peaking between 2 and 5 GHz. In both sources the VLBI jet curves toward the direction of the arcsecond-scale outer jet.

Subject headings: galaxies: jets — interferometry — quasars

I. INTRODUCTION

The superluminal radio sources 3C 273 and 3C 345 have been monitored at 5.0 and 10.7 GHz for many years, and the main features of their expansion are becoming clear (Pearson *et al.* 1981; Unwin *et al.* 1983*a*, hereafter U83). One prominent characteristic is the decay of the "jet" components as they separate from the "core." In both sources the decay time scale is a few years, but the decay is slower, and begins later, at 5.0 GHz than at 10.7 GHz. In both sources the outermost jet component has now become invisible at 10.7 GHz, and we expect that it will similarly fade away at 5.0 GHz within a year or two.

It is important to continue to follow the jet components of these sources as far out as possible to test theories of their origin and motion. If the relativistic beam theory is correct, then many kinematic effects, such as changes in brightness with changes in apparent velocity, should be visible (Blandford and Königl 1979). Since the jet components last longer at lower frequencies, observations at low frequency can be used to follow the components farther out. However, the lower angular resolution makes it harder to separate components, and a range of frequencies must be used. Thus, to complement our studies at higher frequencies, we have made VLBI observations at 2.3 GHz.

II. OBSERVATIONS AND DATA REDUCTION

We made observations of 3C 273 and 3C 345 at 2291 MHz on 1981 November 21, using nine telescopes as a VLBI network. The telescopes are listed in Table 1, with typical system temperatures. We attempted to get nearly complete tracks on all baselines, and the data were very good except for Hartebeesthoek, where recording problems damaged all the data except for part of 3C 273.

The video tapes were correlated on the CIT/JPL MkII processor in Pasadena, and the visibility function was calibrated using the procedure described by Cohen *et al.* (1975). Amplitude errors are dominated by systematic effects, and probably are less than 5%. Errors in closure phase are dominated by random noise. The (u, v) coverage for 3C 273 (Fig. 1*a*) is reasonably uniform but very elongated, and the beam is 6 times longer north-south than east-west. South Africa gave data for 3C 273 to NRAO[1] and the three European stations. As shown in Figure 1*a*, these tracks are short and far from the other tracks; they have little effect on the beam or the final map. 3C 345 (Fig. 1*b*) has gaps at 30 and 50 million wavelengths, but otherwise the coverage is good.

[1]The National Radio Astronomy Observatory is operated by Associated Universities Inc., under contract with the National Science Foundation.

TABLE 1

2.3 GHz VLBI OBSERVATIONS

Station	Diameter (m)	System Temperature (K)
Onsala Space Observatory, Sweden	26	100
Jodrell Bank, UK	26	220
NASA DSS 63, Madrid, Spain	64	25
Hartebeesthoek, South Africa	26	50
NRAO, Green Bank, WV	43	95
George R. Agassiz Station, TX[a]	26	155
Jet Propulsion Laboratory, Pasadena, CA	9	150
Owens Valley Radio Observatory, CA	40	80
Radio Astronomy Laboratory, Hat Creek, CA	26	370

[a]Formerly Harvard Radio Astronomy Station, Fort Davis, Texas.

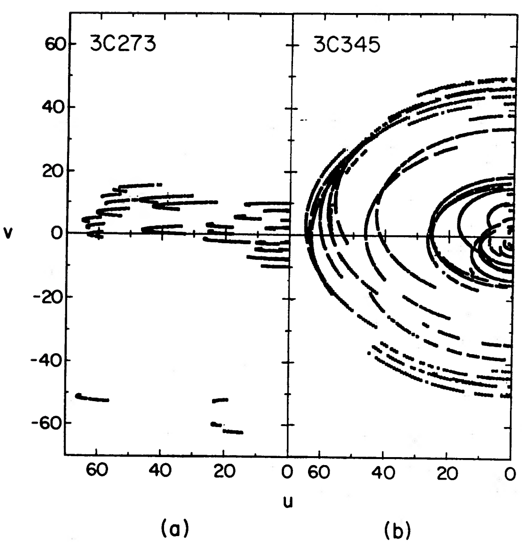

FIG. 1.—Fourier-transform (u, v) plane coverage for the observations of (*a*) 3C 273 and (*b*) 3C 345. Scales are in millions of wavelengths.

We also observed 0235+164 for 5 hr on all baselines, and for a further 5 hr on the US baselines alone. This source is compact, and we had planned to use it as a point source calibrator. However, we could not find a calibration scheme consistent with this assumption, and it was unsuitable as a calibration source. In addition, marginally nonzero closure phases indicated asymmetric structure. An adequate model consists of two point-components of strengths 0.8 ± 0.1 and 0.4 ± 0.1 Jy, separated by 1.4 ± 0.1 milli-arcsec (mas) in position angle (P.A.) $35°\pm5°$. It also is known to be slightly resolved from VLBI experiments at 10.7 GHz (Readhead *et al.* 1980).

Maps were made using the CORTEL algorithm of Cornwell and Wilkinson (1981), which derives self-consistent phases from the closure phases, and telescope-based corrections to the calibration. There were good data on many baselines, and the process converged rapidly for both sources. However, the rms noise on the final maps is substantially greater than expected from receiver noise alone, roughly 20 times greater for 3C 345 and 50 times for 3C 273. Our observations have reasonably good (u, v) coverage, and experience with other interferometers (especially MERLIN, which is similar to a VLBI system) shows that we should be closer to the theoretical noise. We suspect that the problem lies in incorrect amplitude calibrations, and perhaps in baseline-dependent errors. In any event, we believe that there remains room for improvement in the techniques of making maps with VLBI.

III. RESULTS

a) 3C 273

The central region of Figure 1*a* is covered reasonably uniformly, and this allows us to construct a map of 3C 273 smoothed with a circular Gaussian beam of FWHM 10.9 mas, shown in Figure 2*a*. This shows the full area cleaned. The outer contour (± 1%) clearly has systematic distortions, but the 2% contour is substantially correct and represents the source accurately. The high-resolution beam derived from the full coverage in Figure 1*a* was used to derive the map in Figure 2*b*. (The scales in Figs. 2*a* and 2*b* differ by a factor of 2.) There is evidence for five compact components in 3C 273, and we label them from the outside in as C_1, C_2, C_3, C_4, and D, as shown in Figure 2*a* and 2*b*. The three components which are clearly seen, C_2, C_3, and C_4, are definitely resolved east-west and contain substructure. Component C_1, seen in Figure 2*a*, appears as two bumps in Figure 2*b*, but there it is near the limit of dynamic range and

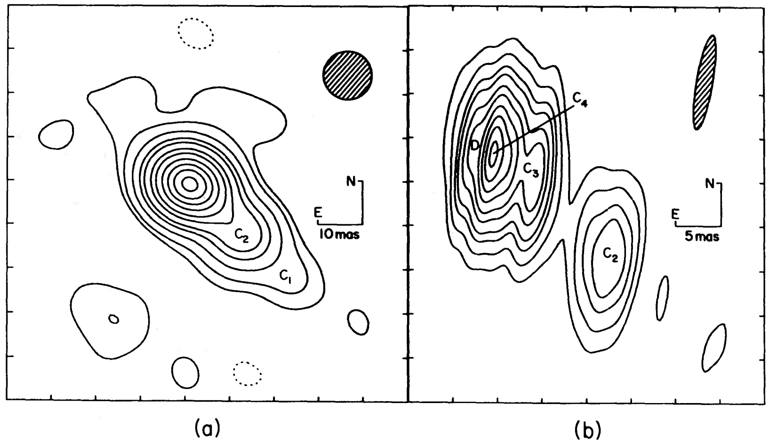

FIG. 2.—Maps of 3C 273 at 2.3 GHz. (*a*) Smoothing beam circular, 10.9 mas diameter (FWHM). Contours at −1, 1, 2, 5, 10, 15, 25, 35, 50, 65, 80, and 95% of peak brightness (19 Jy per beam). Scale 10 mas per tick. (*b*) Smoothing beam 10.9×1.8 mas (FWHM), P.A. = −10°. Contours 2, 5, 10, 15, 25, 35, 50, 65, 80, and 95% of peak brightness (7.3 Jy per beam). Scale 5 mas per tick. Smoothing beams are shown as shaded ellipses.

cannot be trusted. Because the beam is very elongated, none of the components is significantly resolved in the north-south direction; however, the source clearly shows curvature.

Figure 2 may be compared with a number of published maps of 3C 273, including a series at 10.7 GHz by Pearson *et al.* (1981), and one at 5.0 GHz by Readhead *et al.* (1979). Correspondence between the components seen at different frequencies can be made by comparing separations and position angles. There is little danger of misregistration because the source is curved and cannot be shifted lengthwise. The 10.7 GHz maps show components D, C_4, and C_3, while the outer components C_2 and C_1 are too weak to be seen. The 5.0 GHz map (Fig. 2*a* of Readhead *et al.* 1979) shows component C_2 as the two weak outer bumps, which are near the limit of dynamic range and indicate a low-brightness extended structure between 10 and 20 mas from the peak. In the 5.0 GHz map C_3 is the western shoulder on the main peak, and the bright peak is a blend of C_4 and D. The spacing between C_4 and D was about 2 mas in 1977.92 (cf. Fig. 1 of Pearson *et al.* 1981), and the FWHM of the smoothing beam was near 3 mas, so the blending is expected.

A lower resolution map at 0.6 GHz has been published by Wilkinson *et al.* (1979). This shows elongated structure in P.A. ≈ −138°, out to about 40 mas. A clearer view of this outer structure appears in Figure 2*a*, albeit at a higher frequency. The 0.6 GHz map also shows a weak component on the NE side of the nucleus. We have no evidence for that component, to a level of 2%. If it is real, it must have a very steep spectrum.

The spectrum of 3C 273 between 2.3 and 5.0 GHz may be estimated from Figure 3, which shows 2.3 and 5.0 GHz profiles along the ridge of peak brightness. The 5 GHz data are from a 1981.26 map by Unwin *et al.* (1983*b*), smoothed with the 2.3 GHz beam of Figure 4. The two maps were aligned on the peak of C_4. We would have preferred an alignment on D, but at 2.3 GHz, D is too weak and is blended with C_4. At both frequencies the maps appear unresolved across the jet, and the ridge profile gives an adequate measure of flux density. We assume that the components of 3C 273 evolve so slowly that the 7 month separation between the two observations causes only minor errors.

Figure 3 shows that the components have roughly the following spectral indices between 2.3 and 5.0 GHz: $\alpha \approx -1.1$, 0.2, 0.7, 0.3, and 0.2 for components D, C_4, C_3, C_2, and C_1, respectively ($S \sim \nu^{-\alpha}$). The inaccuracy in α is about ± 0.3 except for C_1, where the brightness levels are low and the errors larger. This pattern of spectral index is typical for core-jet sources. At centimeter wavelengths the jet contains components which are optically thin, while the core is optically thick and lies at one end of the jet.

Pearson *et al.* (1981) present maps showing the superluminal separation between components D and C_3, and it is clear that there is rapid separation also between D and C_4. However, C_4 is not well defined on some of the maps, and a quantitative estimate of velocity is not possible. To compare the present observations with their expansion curve, we measure the separation $D - C_3$ at P.A. = −116° and find 8.5 mas for 5.0 GHz and roughly 8 mas for 2.3 GHz. The 5.0 GHz point lies very close to the extrapolated expansion curve, but the 2.3 GHz point lies below the curve but is still consistent with it. This justifies our labeling the east shoulder as component D, in Figure 2*b*.

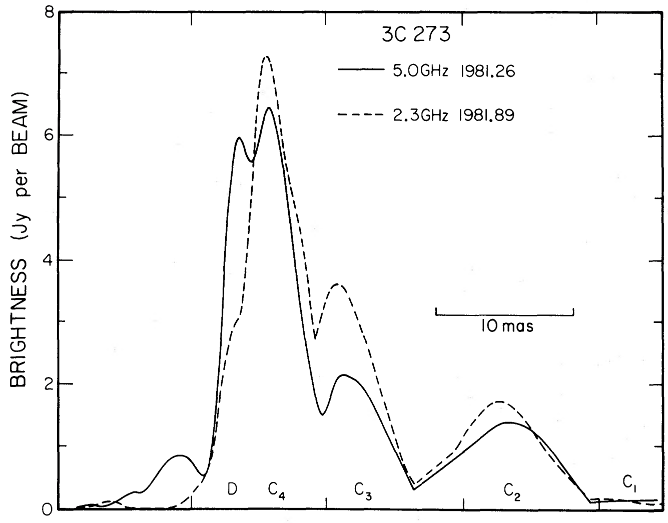

FIG. 3.—Profiles of 3C 273 at 2.3 GHz, epoch 1981.89 (*dashed*) and 5.0 GHz epoch 1981.26 (*solid*), taken at 3 position angles along the ridge of peak brightness. The ridge was defined by P.A. = $-104°$ from the east to the peak of C_4, P.A. = $-116°$ from C_4 to C_3, and P.A. = $-137°$ from C_3 through C_2 and C_1. The smoothing beams in the three sections are 2.0, 3.5, and 6.8 mas (FWHM), respectively. The curves intersect where the spectral index $\alpha = 0$. Abscissa scale 10 mas per tick.

R. S. Simon, A. T. Moffet, and M. H. Cohen (unpublished) made observations of 3C 273 at 2291 MHz in 1978 April. They used three telescopes (Haystack, Green Bank, and Owens Valley) and were able to make a map with limited dynamic range showing three components. Figure 4 shows superposed profiles of the two 2.3 GHz maps, both smoothed with the low-resolution beam. The locations of the components in 1981.89 are indicated above the abscissa. The profiles show two main peaks whose separation increased by 5 ± 2 mas in 3.6 yr, or 1.4 mas per year; however, the main peak in 1981.89 is a superposition of components D, C_4, and C_3, and presumably the same is true of the 1978.3 profile. The proper motion between D and C_2 may be very different from 1.4 mas per year and could be the same as the value found by Pearson *et al.* (1981) for D$-C_3$, 0.76 mas per year.

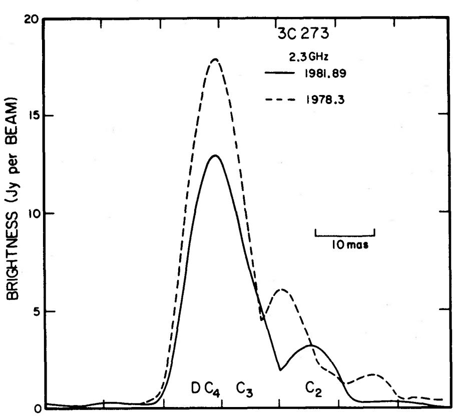

FIG. 4.—Profiles of 3C 273 at 2.3 GHz (peak brightness projected on P.A. = $-116°$). Epochs 1981.89 (*solid*) and 1978.3 (*dashed*). Both maps are smoothed with the large beam of the 1978.3 experiment. Abscissa scale 10 mas per tick.

b) 3C 345

A contour map of 3C 345 at 2.3 GHz is shown in Figure 5. The full area cleaned was substantially bigger than shown in Figure 5, but only one other very small 2% region was found. The region labeled C_1 is larger than any of the others and was the only outlying feature to remain at 2% when the map was smoothed with a bigger beam, and it probably is real.

Figure 5 may be compared with 5.0 GHz maps which have twice the angular resolution: 1980.1 in Spencer *et al.* (1981); 1980.73 in Cohen and Unwin (1982); and 1981.63 in U83. These maps all show three components: the eastern "core" (D) which has an optically thick spectrum with $\alpha \sim -1$ between 5.0 and 10.7 GHz, and inner and outer "jet" components (C_3 and C_2) which are optically thin with $\alpha > 1$ (U83). Figure 5 does not show the unresolved eastern edge seen in all the 5.0 GHz maps, and we attribute this to the blending of components D and C_3, coupled with their differing spectra. In this respect 3C 345 is the same as 3C 273, which we discussed above. The ridge in Figure 5 is curved in the same way as in the 5 GHz maps, and this greatly reduces the ambiguity of registration. The peak of the 2.3 GHz map lies close to C_3 while the weak core (D) shows as an eastward extension. The shoulder to the west is C_2, which is seen as a discrete component at higher frequencies. The outer component in Figure 5, C_1, has not been seen at shorter wavelengths and therefore has a steep spectrum. It presumably is part of the extended structure seen at about the same P.A. at 1.67

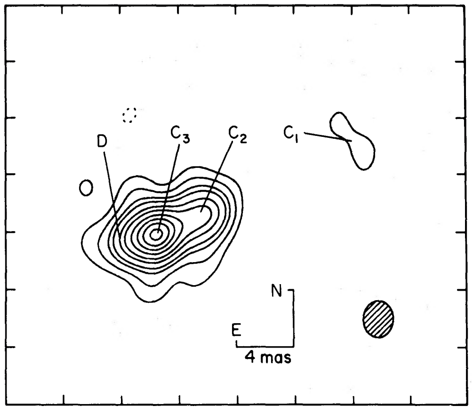

FIG. 5.—Map of 3C 345 at 2.3 GHz. Smoothing beam 2.6×2.1 mas (FWHM), P.A. = −5°. Contours as in Fig. 2*b* (peak brightness 2.2 Jy per beam). Scale 4 mas per tick. Positions of components seen at higher frequency are indicated (see § III*b* for details).

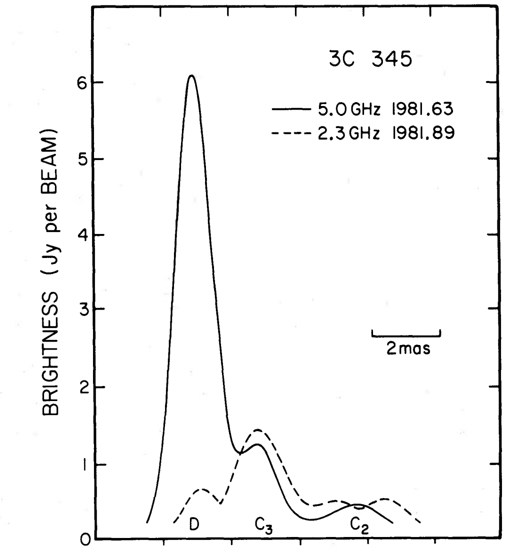

FIG. 6.—Profiles of 3C 345 at 2.3 GHz, epoch 1981.89 (*dashed*) and 5.0 GHz, epoch 1981.63 (*solid*), along P.A. = −79°. The smoothing beam has FWHM = 1.2 mas. The curves intersect where the spectral index is zero. Scale 2 mas per tick.

GHz by Pearson, Readhead, and Wilkinson (1980) and by Stannard *et al.* (1980).

A comparison of Figure 5 with the 5 GHz map made in 1981.63, 3 months earlier (U83, Fig. 1), shows that component D is strongly self-absorbed. To estimate the spectral index of this and the other components, we deconvolved the 2.3 GHz map by two methods. First, we smoothed the δ-functions from CLEAN with the 5 GHz beam, since this allows a direct comparison in brightness units. Secondly, we made a model using the maximum entropy method (MEM) and a program written by S. F. Gull. The two procedures yielded similar solutions, and both models have the same curvature as that in the 5 GHz map.

Figure 6 shows profiles along P.A. = −79° of the 5 GHz map (U83, Fig. 3) and the 2.3 GHz model obtained by smoothing the δ-functions with the 5 GHz beam. The peak at 2.3 GHz was aligned with the peak of the 5 GHz component C_3. This alignment is consistent with the curvature and repeats the procedure used for 3C 273 (Fig. 3). The MEM profile is somewhat smoother than the one shown in Figure 6; the D component is weaker than that shown in Figure 6 by ~ 30%, and the outer C component is single and is stronger by about 30%. Such differences are expected, because models constructed using superresolution are not unique. However, our aim is only to estimate spectral indices. We are certain that there are three major components at 5 GHz, and calculate three spectral indices based on our best estimates of the 2.3 GHz flux.

Spectral indices calculated from Figure 6 are $\alpha = -2.8$, $+0.2$, and $+0.1$ for components D, C_3, and C_2, respectively. The inaccuracy in the index may be ± 0.4, corresponding to a 37% uncertainty in the flux density at 2.3 GHz. The index for the core, $\alpha = -2.8 \pm 0.4$, is comparable with the value expected on the optically thick side of a self-absorbed synchrotron spectrum. Components C_3 and C_2 have flat spectra between 2.3 and 5 GHz, but they are much steeper between 5 and 10.7 GHz, where $\alpha \sim 1$ (U83). This indicates that the jet components C_3 and C_2 have a self-absorption peak between 2 and 5 GHz. The spectral indices are uncertain, but the strong spectral gradient must be correct. The eastern side is very strongly self-absorbed, and the western side is flat. It would be very useful to make the numerical values more precise, especially for the extremely steep spectrum of component D. This can only be done with new observations having higher angular resolution.

IV. DISCUSSION

Our primary objective in these observations was to obtain first-epoch observations at 2.3 GHz so that the superluminal motions could be tracked to larger distances than is possible at shorter wavelengths. A secondary objective was to study the morphology of the sources at an intermediate frequency and relate it to the structures known at other wavelengths. We discuss these in turn.

a) *Superluminal Motion*

In 3C 273 three components seen at 10.7 and 5.0 GHz are also seen at 2.3 GHz, and there is no evidence that their relative positions vary with frequency. As C_4 and C_3 decay and disappear at the high frequencies, we should be able to continue to track them at 2.3 GHz.

In 3C 345 there is insufficient angular resolution to separate the components. The high-resolution model

(Fig. 6) shows many of the features seen at higher frequencies but their reliability is unknown. Observations at several epochs will have to be made before the correspondence between the low and high frequencies is understood. Longer baselines would help greatly in this problem.

The comparison between the 1978.3 and 1981.89 data for 3C 273 illustrates another difficulty caused by inadequate angular resolution. The "components" in Figure 4 are known to be blends of components which probably have independent proper motions and evolutions. This could happen also at higher frequencies. If component D of either 3C 273 or 3C 345 is actually a blend of two or more subcomponents, e.g., a "true" core and a very close inner jet component, then its evolution would be similar to that of the components in the blended "core" in Figure 4, and the measured proper motion could be wrong. The true proper motion would not be much different, however, since the 10.7 and 5.0 GHz proper motions agree, and because the accumulated motion in both sources is much greater than the beamwidth at 10.7 GHz.

b) Morphology and Spectrum

Many compact sources show a linear structure with a bright unresolved "core" at one end of a bumpy curved "jet." This picture must be modified for 3C 273 and 3C 345 at 2.3 GHz because their cores are self-absorbed and weak; the maps show the core only as a shoulder on the first jet component. At low frequencies these sources do not show the characteristic sharp gradient at the core end of the jet.

The core of 3C 345 is very strongly self-absorbed, with $\alpha \approx -2.8 \pm 0.4$, close to the asymptotic low-frequency limit for a uniform incoherent synchrotron cloud. 3C 345 has at least three jet components, and 3C 273 has at least four. They all have rather flat spectra between 2.3 and 5.0 GHz except perhaps C_3 of 3C 273, which has $\alpha \approx 0.7$, and C_1 of 3C 345, which is unknown. The spectral index of the jet components becomes much steeper at higher frequencies.

Distant components, labeled C_1, can be seen in the maps of both sources. These are important, because they trace the jet to a substantial distance. As system improvements are made, the dynamic range will increase; the true shapes of the outer components will then be seen, and it will be possible to track them for proper motions. These outer components have been recognized at lower frequencies, where they are more prominent because of the spectral gradient along the jet. The combination of differing spectra and spacings means that both high and low frequencies are needed to follow the motions of all the components.

Both sources show curvature. This property is very useful because it allows maps made at different epochs and/or wavelengths to be registered with little ambiguity. The curvature of 3C 345 is discussed in two recent articles (Browne *et al.* 1982 and Readhead *et al.* 1983), and the 2.3 GHz data reported here confirm the shape. Because the declination of 3C 273 is low, its curvature is less well determined. Figure 2*b* shows that P.A. $\sim -104°$ at the core, and Figure 2*a* shows that the jet lies at roughly $-133°$. The outer jet (seen at optical and radio wavelengths) lies at P.A. $= -137°$. In 3C 345 the outer jet continues to curve, whereas for 3C 273 it is straight. In 3C 273 the curvature is about 20° in less than 30 pc (projected), and the outer jet is straight from 40 to 80 kpc (projected); there is further curvature of about 4° at an intermediate distance.

We are grateful to the many people involved with the US and European VLBI Networks, under whose auspices this work was done. We thank A. C. S. Readhead for comments on the manuscript, and J. Biretta for help with the maximum entropy mapping. M. H. C. is grateful to the John Simon Guggenheim Memorial Foundation and the Institute of Astronomy, Cambridge, for their assistance during the initial phase of this work. The US VLBI Network is supported by NSF, and the work at JPL and DSS 63 is supported by NASA under contract NAS 7-100.

REFERENCES

Blandford, R. D., and Königl, A. 1979, *Ap. J.*, **232**, 34.
Browne, I. W. A., Clark, R. R., Moore, P. K., Muxlow, T. W. B., Wilkinson, P. N., Cohen, M. H., and Porcas, R. W. 1982, *Nature*, **299**, 788.
Cohen, M. H., *et al.* 1975, *Ap. J.*, **201**, 249.
Cohen, M. H., and Unwin, S. C. 1982, in *IAU Symposium 97, Extragalactic Radio Sources*, ed. D. S. Heeschen and C. M. Wade (Dordrecht: Reidel), p. 345.
Cornwell, T. J., and Wilkinson, P. N. 1981, *M.N.R.A.S.*, **196**, 1067.
Pearson, T. J., Readhead, A. C. S., and Wilkinson, P. N. 1980, *Ap. J.*, **236**, 714.
Pearson, T. J., Unwin, S. C., Cohen, M. H., Linfield, R. P., Readhead, A. C. S., Seielstad, G. A., Simon, R. S., and Walker, R. C. 1981, *Nature*, **290**, 365.
Readhead, A. C. S., Hough, D. H., Ewing, M. S., Walker, R. C., and Romney, J. D. 1983, *Ap. J.*, **265**, 107.
Readhead, A. C. S., Pearson, T. J., Cohen, M. H., Ewing, M. S., and Moffet, A. T. 1979, *Ap. J.*, **231**, 299.
Readhead, A. C. S., Walker, R. C., Pearson, T. J., and Cohen, M. H. 1980, *Nature*, **295**, 137.
Spencer, J. H., Johnston, K. J., Pauliny-Toth, I. I. K., and Witzel, A. 1981, *Ap. J.* (*Letters*), **251**, L61.
Stannard, D., Booth, R. S., Spencer, R. E., and Bååth, L. B. 1980, *M.N.R.A.S.*, **192**, 555.
Unwin, S. C., Cohen, M. H., Pearson, T. J., Seielstad, G. A., Simon, R. S., Linfield, R. P., and Walker, R. C. 1983*a*, *Ap. J.*, **271**, 536 (U83).
Unwin, S. C., Cohen, M. H., Biretta, J. A., Pearson, T. J., Seielstad, G. A., Simon, R. S., Linfield, R. P., and Walker, R. C. 1983*b*, *Ap. J.*, in preparation.
Wilkinson, P. N., Readhead, A. C. S., Anderson, B., and Purcell, G. H. 1979, *Ap. J.*, **232**, 365.

R. S. BOOTH: Onsala Space Observatory, S-439 00 Onsala, Sweden

M. H. COHEN, K. R. LIND, A. T. MOFFET, R. S. SIMON, and S. C. UNWIN: Owens Valley Radio Observatory, California Institute of Technology, Mail Code 105-24, Pasadena, CA 91125

G. D. NICOLSON: National Institute for Telecommunications Research, P.O. Box 3718, Johannesburg 2000, South Africa

A. E. NIELL and L. E. YOUNG: Jet Propulsion Laboratory, 4800 Oak Grove Drive, Pasadena, CA 91109

R. S. SIMON: E. O. Hulburt Center for Space Research, Naval Research Laboratory, Code 41345, Washington, DC 20375

R. E. SPENCER and P. N. WILKINSON: Nuffield Radio Astronomy Laboratories, Jodrell Bank, Macclesfield, Cheshire SK11 9DL, UK